

Satratoxin-G from the Black Mold *Stachybotrys chartarum* Induces Rhinitis and Apoptosis of Olfactory Sensory Neurons in the Nasal Airways of Rhesus Monkeys

STEPHAN A. CAREY^{1,2}, CHARLES G. PLOPPER³, DALLAS M. HYDE⁴, ZAHIDUL ISLAM^{2,5},
JAMES J. PESTKA^{2,5}, AND JACK R. HARKEMA^{2,6}

¹Department of Small Animal Clinical Sciences, College of Veterinary Medicine, Michigan State University, East Lansing, Michigan, USA

²Center for Integrative Toxicology, Michigan State University, East Lansing, Michigan, USA

³Department of Anatomy, Physiology, and Cell Biology, School of Veterinary Medicine, University of California–Davis, Davis, California, USA

⁴California National Primate Research Center, University of California–Davis, Davis, California, USA

⁵Department of Food Science and Human Nutrition Michigan State University, East Lansing, Michigan, USA

⁶Department of Pathobiology and Diagnostic Investigation, College of Veterinary Medicine, Michigan State University, East Lansing, Michigan, USA

ABSTRACT

Satratoxin-G (SG) is a trichothecene mycotoxin of *Stachybotrys chartarum*, the black mold suggested to contribute etiologically to illnesses associated with water-damaged buildings. We have reported that intranasal exposure to SG evokes apoptosis of olfactory sensory neurons (OSNs) and acute inflammation in the nose and brain of laboratory mice. To further assess the potential human risk of nasal airway injury and neurotoxicity, we developed a model of SG exposure in monkeys, whose nasal airways more closely resemble those of humans. Adult, male rhesus macaques received a single intranasal instillation of 20 µg SG (high dose, $n = 3$), or 5 µg SG daily for four days (repeated low dose, $n = 3$) in one nasal passage, and saline vehicle in the contralateral nasal passage. Nasal tissues were examined using light and electron microscopy and morphometric analysis. SG induced acute rhinitis, atrophy of the olfactory epithelium (OE), and apoptosis of OSNs in both groups. High-dose and repeated low-dose SG elicited a 13% and 66% reduction in OSN volume density, and a 14-fold and 24-fold increase in apoptotic cells of the OE, respectively. This model provides new insight into the potential risk of nasal airway injury and neurotoxicity caused by exposure to water-damaged buildings.

Keywords: stachybotrys; olfactory toxicity; rhesus monkeys; trichothecene; mycotoxin.

INTRODUCTION

Damp building–related illnesses (DBRI) include a myriad of respiratory, immunologic, and neurologic symptoms (Anderson et al. 1997) associated with exposure to damp indoor air environments resulting from extreme condensation, failure of water-use devices, or building envelope breach during heavy rains and flooding (Institute of Medicine 2004). DBRI are frequently linked to aberrant indoor growth of fungi (Fog Nielsen

2003), one of which is *Stachybotrys chartarum*, a black pigmented, saprophytic fungus that grows on water-damaged cellulosic building materials (Fung et al. 1998; Hossain et al. 2004; Kilburn 2004; Tuomi et al. 2000). In 2004, an Institute of Medicine (IOM) expert panel concluded that there is sufficient evidence for an association between damp building exposure and lower airway symptoms such as wheeze, cough, and exacerbation of chronic lower airway diseases (e.g., asthma). However, this panel also concluded that supportive data for other reported outcomes such as neurocognitive dysfunction, mucous membrane irritation, and immune disorders are lacking. It was further suggested that while existing *in vitro* and *in vivo* research on *S. chartarum* and its mycotoxins indicate adverse effects in humans are “biologically plausible,” their association with DBRI requires rigorous validation from the perspectives of mechanisms, dose response, and exposure assessment.

The satratoxins, macrocyclic trichothecenes produced by *S. chartarum*, are translational inhibitors that initiate both inflammatory gene expression and apoptosis *in vitro* following upstream activation of mitogen-activated protein kinases (Chung et al. 2003; Yang et al. 2000). Satratoxin equivalent

This work was supported by the National Institutes of Health, National Center for Research Resources P51 RR000169.

Address correspondence to: Stephan A. Carey, Department of Small Animal Clinical Sciences, College of Veterinary, Michigan State University, Room 242 Food Safety and Toxicology Building, East Lansing, MI 48824, USA; e-mail: careys@msu.edu.

Abbreviations: BG, Bowman’s glands; CNPRC, California National Primate Research Center; DBRI, damp building–related illnesses; EDTA, ethylenediaminetetraacetic acid; H&E, hematoxylin and eosin; IOM, Institute of Medicine; NALT, nasal associated lymphoid tissue; NB, olfactory nerve bundle; OE, olfactory epithelium; OMP, olfactory marker protein; ON, olfactory nerve; OSN, olfactory sensory neuron; PMN, polymorphonuclear leukocyte; SC, sustentacular cell; SG, satratoxin-G; TEM, transmission electron microscopy; Vs, volume density.

airborne concentrations ranging from 2 to 34 ng/m³ (Yike et al. 1999) and 54 to 330 ng/m³ (Vesper et al. 2000) have been previously estimated to occur in rooms of water-damaged homes heavily contaminated with *Stachybotrys*. These water-soluble mycotoxins occur in the outer plasmalemma surface and the inner wall layers of conidiospores (Gregory et al. 2004) as well as in nonviable airborne particulates (Brasel et al. 2005), which could facilitate entry and release in the respiratory tract. Pulmonary toxicity induced by the spores of *S. chartarum* and associated trichothecenes has been demonstrated in laboratory rodents following intranasal or intratracheal exposure (Yike and Dearborn 2004; Yike et al. 2005).

The nasal passages have been described as an efficient “scrubbing tower” for the respiratory tract because they effectively absorb water-soluble and reactive gases and vapors, trap inhaled particles, and metabolize airborne xenobiotics (Brain 1970). These protective functions also make the nose vulnerable to acute or chronic injury caused by exposure to airborne toxic agents. Our research group has reported that acute intranasal exposure to satratoxin G (SG) induces widespread apoptosis of olfactory sensory neurons (OSNs) in the olfactory epithelium (OE), with an accompanying acute, neutrophilic rhinitis, in the nasal airways of laboratory mice (Islam et al. 2006). Recently, SG exposure has been demonstrated to impair olfactory function in mice (Jia et al. 2011). Accordingly, these findings suggest that rhinitis and neurotoxicity are potential adverse health effects of inhalational exposure to black mold in the indoor air of water-damaged buildings.

While these reported findings in rodent models are concerning, structural and functional differences between the olfactory systems of rodents and primates make it challenging to extrapolate human risk from rodent studies. Rodents are obligate nasal breathers, have complex folding and branching patterns to their nasal turbinates, and have extensive amounts of olfactory epithelium covering approximately 50% of their nasal airways. In contrast, macaque monkeys and humans are oronasal breathers, have simple turbinate structures (Harkema et al. 2006), and have olfactory epithelium confined to a small region in the superior aspect of the nasal cavity (Figure 1), comprising less than 15% of their total nasal surface area (Carey et al. 2007). To determine whether these structural differences alter the potential for nasal toxicity and neurotoxicity caused by SG and *Stachybotrys*, we developed an experimental model of acute and repeated intranasal SG exposure in the young adult rhesus monkey, whose nasal airways and olfactory system more closely mimic those of humans. We hypothesized that intranasal exposure of SG evokes apoptosis of OSNs and acute inflammation in the nasal airways of monkeys, similar to that previously observed in laboratory mice (Islam et al. 2006). The current study aimed to determine the susceptibility of the nasal airways of the rhesus monkey to acute SG-induced injury, and to compare the effects of single and repeated intranasal exposures to SG on the induction of toxic nasal airway injury and inflammation.

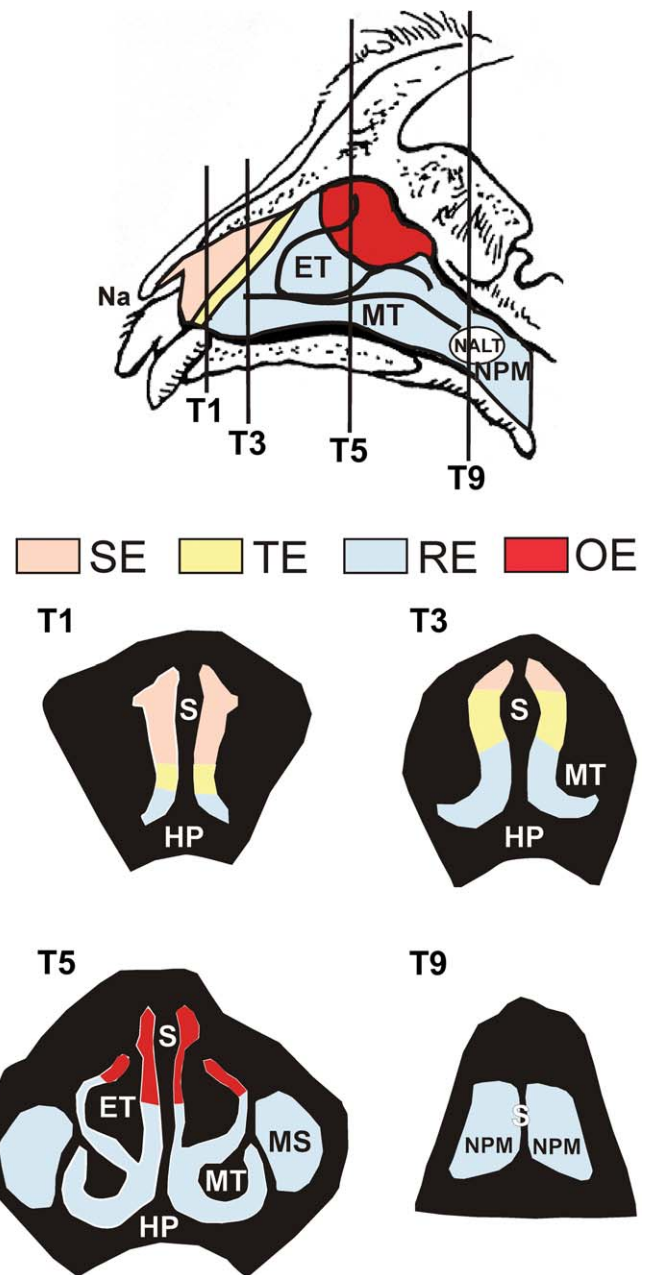


FIGURE 1.—Diagrammatic representation of the nasal passages of the rhesus monkey. Distribution of the nasal surface epithelia covering the right nasal lateral wall and turbinates of the rhesus monkey. The vertical lines indicate the locations of the transverse sections T1, T3, T5, and T9. Cross-sectional views of these four sections are diagrammed below. Color coding indicates the regions of the nasal airways lined by squamous epithelium (SE), non-ciliated transitional epithelium (TE), respiratory epithelium (RE), and olfactory epithelium (OE). The entire surface of the right lateral wall, nasal septum (S), and ethmoturbinate (ET) lined by OE exhibited apoptosis of olfactory sensory neurons, atrophy, and acute rhinitis following both high-dose and repeated low-dose exposure to SG. NALT = nasal-associated lymphoid tissue; NPM = nasopharyngeal meatus; MT = maxilloturbinate; HP = hard palate; MS = maxillary sinus.

TABLE 1.—Extrapolation of Satratoxin-G dose from the mouse to the monkey.

	Mouse	Monkey
Dose SG per nasal passage	1 μg ^a	20 μg
Area of nasal passage	150 mm^2 ^b	3000 mm^2 ^b
Percentage of nasal passage lined by OE	50%	15%
Area of OE per nasal passage	75 mm^2	450 mm^2
Dose of SG delivered to OE (total dose * % OE)	500 ng	3000 ng
Dose of SG per mm^2 OE	500 ng SG / 75 mm^2 OE \approx 6.7 ng/ mm^2	3,000 ng SG / 450 mm^2 OE \approx 6.7 ng/ mm^2

^a Extrapolation is based on a 100 $\mu\text{g}/\text{kg}$ dosage of SG (Islam et al. 2006), divided equally into each nasal passage of a 50 g mouse.

^b Nasal cavity morphometric estimates taken from Gross and Morgan (1991).

MATERIALS AND METHODS

Animals and Intranasal Exposure

Six male, 2- to 3-year-old rhesus monkeys (*Macaca mulatta*) were used in this study. All monkeys were obtained from the breeding colony at the California National Primate Research Center (CNPRC) at the University of California, Davis. Care and housing of the animals before, during, and after treatment complied with the provisions of the Institute of Laboratory Animal Resources and conformed to practices established by the American Association for Accreditation of Laboratory Animal Care. All animal protocols were reviewed and approved by the University of California, Davis, Institutional Animal Care and Use Committee.

Since the surface area of one nasal passage in the young, adult male rhesus monkey nasal airway (3,000 mm^2) is approximately 20 times greater than that in the young adult, male C57/Bl6 mouse (150 mm^2) (Gross and Morgan 1991), we selected a total intranasal dose of SG in the monkey (20 μg per nasal passage) that was a comparable concentration of SG per mm^2 of OE to that previously shown to cause nasal toxicity in the mouse (1 μg per nasal passage or 100 $\mu\text{g}/\text{kg}$ bw) (Islam et al. 2006) (Table 1). For intranasal instillations, monkeys were lightly anesthetized with ketamine (5–10 mg/kg, IM) and medetomidine (20–30 μg IM) in order to safely conduct the instillations without physical restraint. Three of the monkeys in this study were treated with a single, intranasal instillation of 20 μg SG in 0.5 ml saline in the right nasal passage (single, high-dose) using a microsyringe (Penn-Century, Inc., Philadelphia, PA) that delivered a plume of liquid aerosol (16–22 μm mass mean diameter particles) throughout the nasal cavity. The left nasal passage was similarly instilled with saline vehicle alone (0.5 ml) to serve as an internal control. The other 3 monkeys received a single, daily intranasal instillation of 5 μg SG in 0.5 ml saline in the right nasal passage, and saline vehicle in the left nasal passage, each day for 4 consecutive days (repeated, low-dose). At the end of each exposure, all animals were treated with atipamezole (0.15 mg/kg IM) as a medetomidine reversal agent.

Necropsy and Tissue Preservation

Twenty-four hours after the last intranasal instillation, each monkey was anesthetized with ketamine (10 mg/kg IM) and

euthanized via exsanguination by a CNPRC veterinarian. Immediately after euthanasia, the head was removed from the carcass, and the lower jaw, skin, and musculature was removed from the head. Each nasal passage was flushed retrograde through the nasopharyngeal meatus with 5 ml of a 1% paraformaldehyde and 0.1% glutaraldehyde fixative solution, followed by immersion in 250 ml of the same solution for at least 24 hours at 4°C until further processing for light and transmission electron microscopy (TEM).

Tissue Processing for Light and Electron Microscopy

Each nasal cavity specimen was removed from the fixative solution and decalcified in 500 ml of 10% ethylenediaminetetraacetic acid (EDTA) in 0.1 M sodium cacodylate, pH 7.4, for 120 days and then rinsed with distilled water for 2 to 4 hours. After decalcification, the nasal cavity was transversely sectioned at 10 specific anatomic locations from the rostral nasal vestibule (T-1) to the caudal nasopharyngeal meatus (T-10) in a plane perpendicular to the hard palate and nasal septum using gross dental and palatine landmarks, in a manner similar to a previously described method (Carey et al. 2007).

One transverse section (T-5) was selected for processing for TEM to examine the ultrastructure of the olfactory epithelium. This section was selected because it included profiles of the dorsal nasal septum and the dorsal ethmoturbinate, regions known to be lined with olfactory epithelium. Within this section, mucosal samples from the dorsal third of the nasal septum and dorsal ethmoturbinate on the left (saline) and right (SG) nasal passage were dissected and postfixed in 1% osmium tetroxide, dehydrated through a graded series of ethanol and propylene oxide solutions, and embedded in Poly/Bed-Araldite resin (Polysciences, Inc., Warrington, PA). Semithin sections (1 μm) were cut and stained with toluidine blue for light microscopic identification of tissue sites for TEM. Ultrathin tissue sections for TEM were cut at approximately 75 nm with a diamond knife, mounted on copper grids, and stained with lead citrate and uranyl acetate. Sectioning was done with an LKB Ultratome III (LKB Instruments, Inc., Rockville, MD). Ultrastructural tissue examination and photography were performed with a JEOL JEM 100CXII electron microscope (JEOL Ltd., Tokyo, Japan).

The remaining nine transverse sections were processed for light microscopic examination. All sections were split

sagittally, 1–2 mm to the left of midline. This sectioning provided a complete right nasal section with both saline (left) and SG (right) sides of the septum attached, and a free left lateral wall at each level. Sections were embedded in paraffin with the anterior face sectioned at a thickness of 5 μm , and stained with hematoxylin and eosin. All sections were examined for routine histopathology and identification of olfactory mucosa.

Immunohistochemistry

Additional 5 μm paraffin sections were obtained from all tissue blocks containing profiles of olfactory mucosa. Unstained and hydrated paraffin sections were treated with 3% hydrogen peroxide in methanol to destroy endogenous peroxidase, followed by incubation with a nonspecific protein-blocking solution containing normal sera (Vector Laboratories, Inc., Burlingame, CA), an endogenous avidin-blocking solution (Vector Laboratories), and an endogenous biotin blocking solution (Sigma-Aldrich, St. Louis, MO). Blocked sections were incubated with specific dilutions of primary polyclonal antibodies directed against activated caspase-3 (1:30, overnight at 4°C, rabbit anti-caspase-3 antibody; Abcam, Inc., Cambridge, MA), olfactory marker protein (OMP; 1:2,000, overnight at 4°C, goat anti-OMP antibody, provided by F. Margolis, University of Maryland), and myeloperoxidase (1:250, 60 minutes at room temperature, rabbit anti-human granulocytic myeloperoxidase antibody; Lab Vision Corporation, Fremont, CA) for immunohistochemical identification of neutrophils. All primary antibodies were followed by the secondary antibody, biotinylated anti-species IgG (Vector Laboratories). Immunoreactivity was visualized with Vectastain R.T.U. Elite ABC-Peroxidase Reagent followed by Nova Red (Vector Laboratories) as the chromagen. After immunohistochemical staining, slides were counterstained with hematoxylin.

Light Microscopic Morphometry

Thickness of the OE and the volume density of OMP-positive OSNs in the OE lining the dorsal third of the T-5 section were morphometrically estimated as previously described for airway epithelium (Hyde et al. 1991, 1990; Plopper et al. 1994), and as previously utilized for olfactory epithelium in mice (Islam et al. 2006). This region was identified by measuring the length of the entire nasal septum in the T-5 (right) section, dividing this length by three, and measuring this distance along the septum from the apex of the dorsal meatus. The septal length was calculated from the contour length of the basal lamina on a digitized image, using image analysis software (Scion Image, Scion Corporation, Frederick, MD). All measurements were obtained at a final magnification of 1,710x using a light microscope (Olympus BX40; Olympus America, Inc., Melville, NY) coupled to a 3.3-megapixel digital color camera (Q-Color 3 Camera; Quantitative Imaging Corporation, Burnaby, British Columbia, Canada), and a personal computer (Dimension 8200; Dell, Austin, TX). The morphometric analyses were performed using a

135-point cycloid grid overlay with an automated software package for counting points and intercepts within the grid (Stereology Toolbox; Morphometrix, Davis, CA) (Hyde et al. 1991, 1990). The percent volume density (the proportion of the total epithelial volume), V_v , of OMP-positive OSNs was determined by point counting and calculated using the following formula:

$$V_v = P_p = P_n/P_t, \quad (1)$$

where P_p is the point fraction of P_n , the number of test points hitting OMP-immunoreactive OSNs, divided by P_t , the total number of points hitting the reference space (i.e., olfactory epithelium). The volume of each epithelial component of interest per unit of basal lamina length (S_v) was determined by point- (epithelial component) and intercept- (basal lamina) counting and was calculated using the following formula:

$$S_v = 2I_oL_\gamma, \quad (2)$$

where I_o is the number of cycloid intercepts with the object (epithelial basal lamina), and L_γ is the length of the test line in the reference volume (epithelium within the test grid). To determine the thickness of the OE, a volume per unit area of basal lamina (cubic micrometers per square micrometer) was calculated using the following formula for arithmetic mean thickness (τ):

$$\tau = V_V/S_V. \quad (3)$$

Other standard morphometric and image analysis techniques were used to estimate the numeric cell density of intraepithelial polymorphonuclear neutrophils and apoptotic OSNs in the OE in this region. Neutrophil numeric densities were determined by counting the number of nuclear profiles of neutrophils within the OE, and dividing this number by the total length of the basal lamina underlying the epithelium in this region. Neutrophils were identified on the basis of characteristic, multilobed nuclear morphology, and cytoplasmic myeloperoxidase immunoreactivity. The apoptotic OSN numeric density was similarly estimated by counting the total number of caspase-3-immunoreactive OSN profiles in the OE, and dividing this number by the length of the basal lamina, calculated as described above.

Statistical Analyses

Comparisons of morphometric data within a dosing scheme (i.e., left side vs. right side within the same animal) were analyzed using paired Student's *t*-test for dependent samples. Comparisons across dosing schemes (1-day SG vs. 4-day SG) were analyzed using Student's *t*-test for independent samples. Results are displayed as group means \pm SEM. The criterion for statistical significance was set at $p \leq 0.05$. All statistical analyses were performed using a commercial statistical software package (SigmaStat, SPSS Science, Chicago, IL).

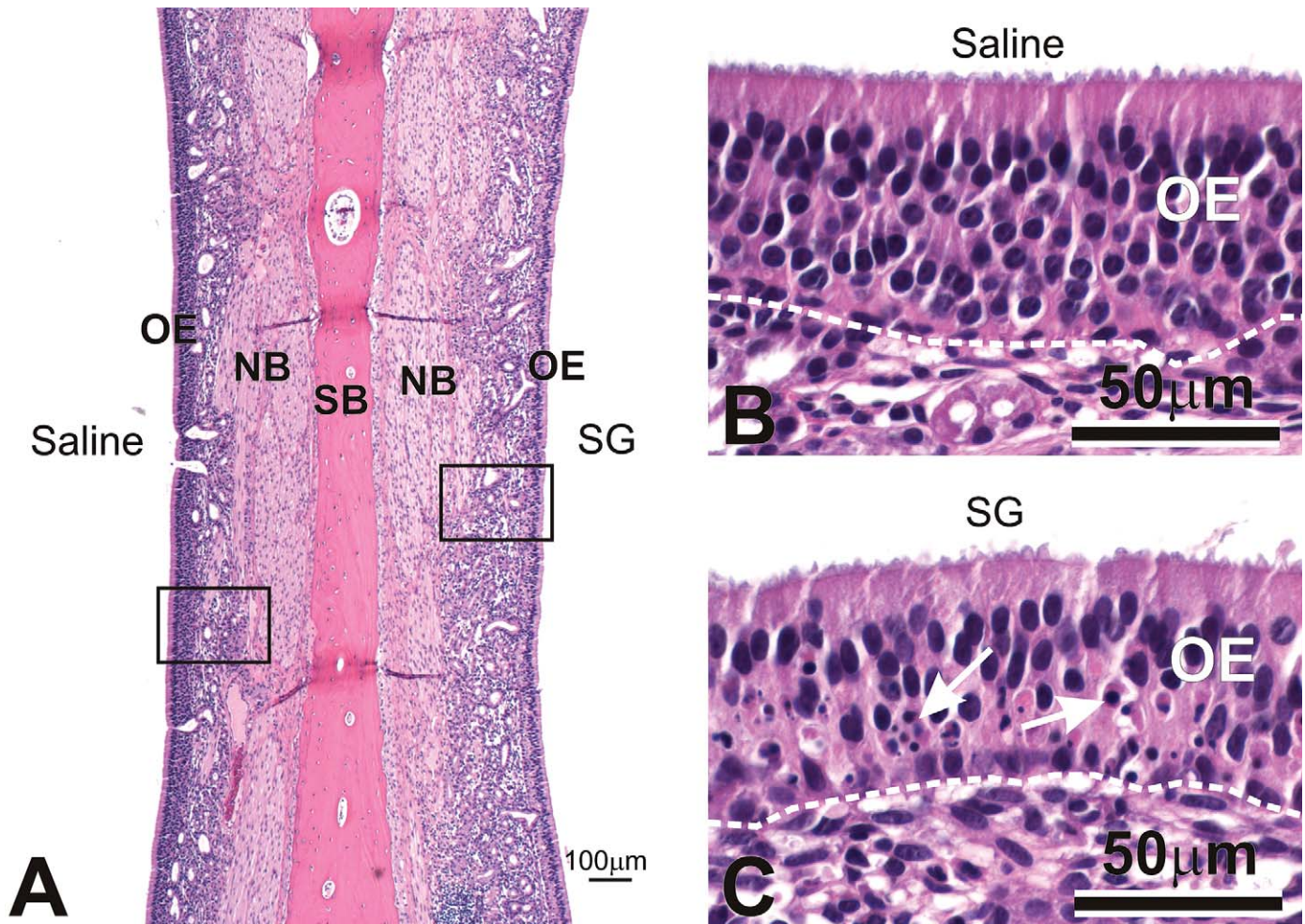


FIGURE 2.—SG-induced atrophy of olfactory epithelium. (A, B, C) Photomicrographs of the olfactory epithelium (OE) lining the dorsal nasal septum of a rhesus monkey treated with saline alone in the left nasal passage (A, B), and repeated low-dose SG (5 $\mu\text{g}/\text{day}$ \times 4 days) in the right nasal passage (A, C). Note the presence of apoptotic OSN nuclei (arrows) and epithelial atrophy in the SG-exposed nasal passage (C). NB = olfactory nerve bundles; SB = septal bone. Dashed line = basal lamina. Tissues stained with hematoxylin and eosin.

RESULTS

Nasal Histopathology

Histopathological examination of the nine transverse sections processed for light microscopy revealed similar inflammatory and epithelial lesions in the nasal passages exposed to a single dose of 20 μg (high-dose) SG and those exposed to 4 consecutive daily doses of 5 μg (repeated low-dose) SG. In both groups, these lesions were confined primarily to all regions of the olfactory mucosa, including the dorsal nasal septum, the dorsal portion of the ethmoturbinate, and the dorsal lateral wall, in monkeys from both SG dose groups (Figure 1). No inflammatory alterations were observed in the saline-exposed nasal passages, or in the squamous or transitional epithelial mucosa of the SG-exposed nasal passages. In H&E-stained sections, olfactory sensory neurons in all SG-exposed nasal passages exhibited morphologic features consistent with apoptosis, including condensed cell bodies; clumped, fragmented nuclear material; and scattered, basophilic cellular

fragments (apoptotic bodies). Apoptosis of OSNs was present in all regions of olfactory mucosa but was locally extensive in the olfactory epithelium lining the middle and dorsal nasal septum (Figure 2). No morphologic evidence of OSN apoptosis was evident on H&E-stained sections from any of the saline-exposed nasal passages. Concurrent with the SG-induced OSN apoptosis was a mild decrease in the height of the olfactory epithelium in the nasal airways exposed to both high-dose and repeated low-dose SG. This OE atrophy was associated with a reduction in the height of the OSN layer, and an accompanying decrease in the height of the surrounding sustentacular cells. Sustentacular cells and basal cells in the nasal airways of both SG-exposed groups were otherwise morphologically normal.

Intranasal exposure to SG also induced a marked, acute rhinitis in the nasal airways of monkeys from both high-dose and repeated, low-dose exposure groups. This rhinitis was similar in magnitude and distribution in both exposure groups, and consisted primarily of an infiltration of polymorphonuclear leukocytes (neutrophils) into the epithelium and lamina propria

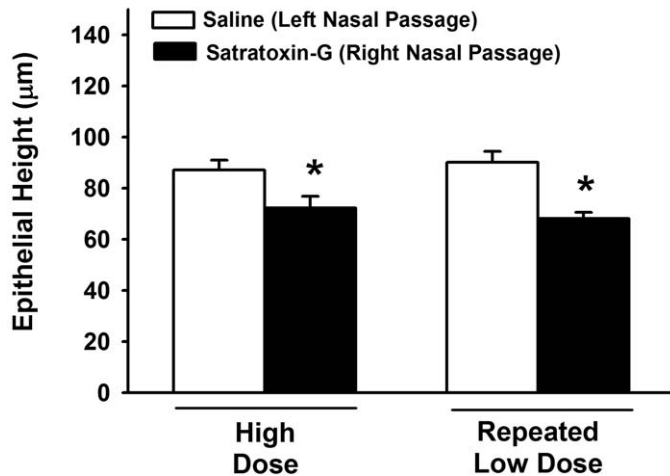


FIGURE 3.—Morphometric analysis of epithelial thickness (atrophy). * = significantly different from respective saline-exposed group.

of the olfactory mucosa. Within the lamina propria, this rhinitis was locally extensive in the immediate subepithelial space surrounding olfactory nerve bundles and Bowman's glands. Neutrophilic inflammation was largely confined to the olfactory mucosa, but was also present to a lesser extent in regions of respiratory epithelium immediately adjacent to the OE. Neutrophils were also present in the airway lumen overlying the OE along the nasal septum and were frequently admixed with airway mucus and degenerating, exfoliated epithelial cells, and cellular debris.

Morphometric Estimation of Epithelial Atrophy

Morphometry of the OE lining the dorsal third of the nasal septum confirmed that intranasal SG-exposure caused a reduction in overall OE height at 24 hours following both high-dose (17% reduction) and repeated, low-dose (24% reduction) exposures, relative to the height of the OE in the respective saline-exposed nasal passage (Figure 3). There was no significant difference in the overall height of the OE, or in the change in OE height (compared to respective controls) between high-dose and repeated low-dose groups.

Depletion of OSNs in SG-Exposed OE

Sections of OE from the dorsal septum were immunohistochemically stained for the detection of OMP, a cell-specific peptide found only in mature OSNs (Kream and Margolis 1984). OMP immunoreactivity was observed in the OSN cell bodies in the middle layer of the OE, in the dendritic terminations of OSNs along the apical surface of the OE, and within the olfactory nerve bundles within the lamina propria of the olfactory mucosa of the saline-exposed nasal passages (Figure 4). High-dose SG exposure caused a moderate decrease in OMP immunoreactivity in all regions of OE. This loss was observed primarily in the OSN layer and intraepithelial axons of the OE, while immunoreactivity in the olfactory nerve bundles of the lamina propria was largely maintained. In contrast,

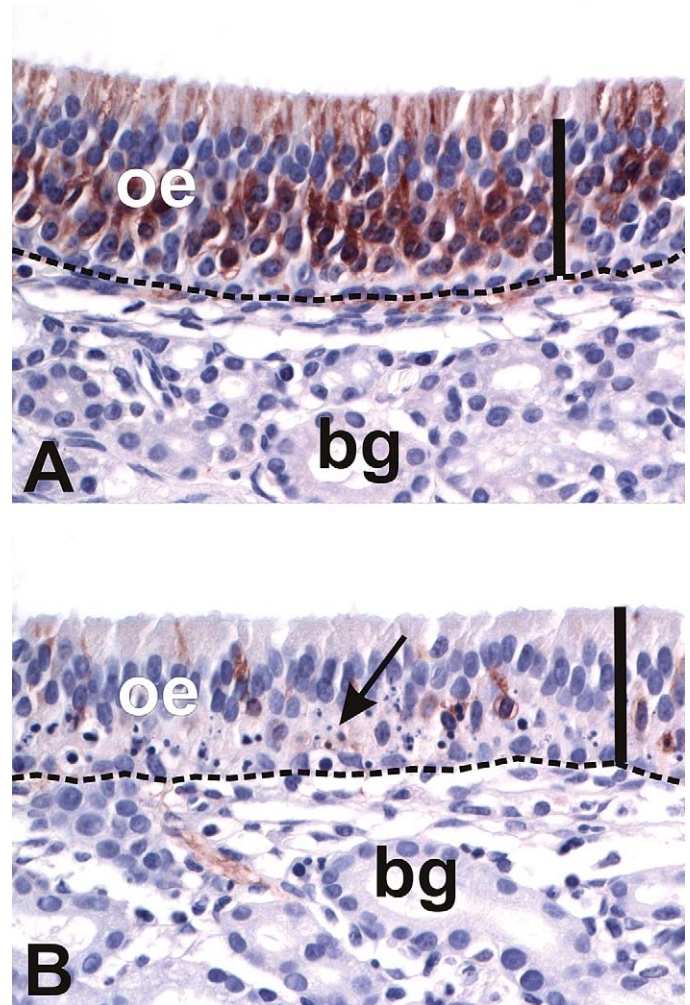


FIGURE 4.—SG-exposure depletes OSNs in olfactory epithelium (OE). (A, B) Light photomicrographs of OE lining the dorsal nasal septum of a rhesus monkey treated with saline alone in the left nasal passage (A) and repeated low-dose SG in the right nasal passage (B). Sections were immunohistochemically stained with anti-olfactory marker protein (OMP) antibody and counterstained with hematoxylin. Immunoreactivity for OMP (marker for mature olfactory sensory neurons) is identified by the brown chromagen in the OE. Note the presence of apoptotic OSN nuclei (arrows) and the loss of OMP immunoreactivity in the SG-exposed nasal passage (B). Scale bars = 50 µm. Dashed line = basal lamina. bg = Bowman's glands.

repeated low-dose SG exposure markedly reduced both intraepithelial and olfactory nerve OMP staining, with focal areas of complete loss of intraepithelial OMP staining along the dorsal nasal septum (Figure 4). Morphometric analysis revealed a 13% and 66% reduction in the volume density of OMP-positive OSNs in the OE of nasal passages exposed to high-dose and repeated low-dose SG, respectively (Figure 5).

Induction of OSN Apoptosis in SG-Exposed OE

Both high-dose and repeated low-dose SG exposures induced apoptosis in the olfactory mucosa. Apoptosis was

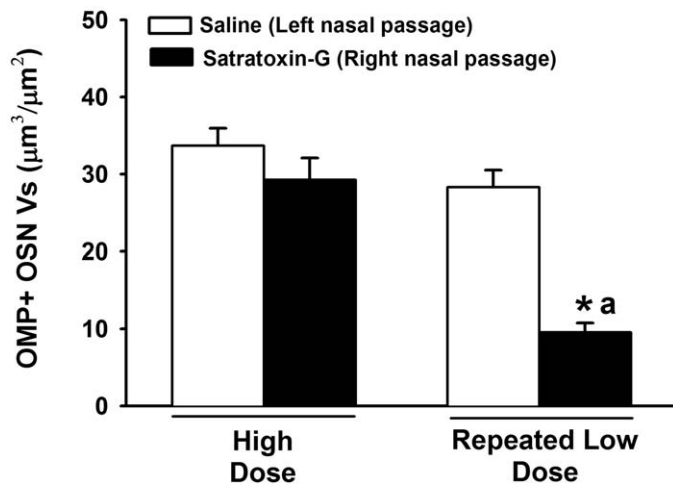


FIGURE 5.—Morphometric analysis of volume density (V_s) of OMP-positive olfactory sensory neurons in the OE lining the dorsal nasal septum. * = significantly different from respective saline-treated group. a = significantly different from high-dose SG-treated group.

confined to the OSN in the OE and the olfactory nerves in the lamina propria. Since the trichothecene mycotoxins are capable of inducing apoptosis via activation of either the intrinsic or extrinsic pathways (Yang et al. 2000), tissues were immunohistochemically analyzed for activated caspase-3, the inducible effector caspase common to both apoptotic pathways. Apoptotic OSNs expressed activated caspase-3 in the cell bodies and axons of the OE. Activated caspase-3 expression was also detected in the OSN axons within the olfactory nerve bundles in the underlying lamina propria (Figure 6). The numeric density of OSNs expressing activated caspase-3 within the OE lining the dorsal septum was 14-fold higher following high-dose SG exposure, and 24-fold higher following repeated low-dose SG exposure, compared to their respective saline exposed nasal passages (Figure 7).

Morphometry of Neutrophilic Inflammation in OE

All SG-exposed nasal passages (high-dose and repeated low-dose) exhibited neutrophilic rhinitis within the olfactory epithelium lining the dorsal nasal septum (Figure 8). Both high-dose SG and repeated low-dose SG exposure resulted in a 9-fold increase in intraepithelial neutrophils in the OE lining the dorsal septum, compared to the dorsal septal OE in saline-exposed nasal passages. There was no significant difference in the magnitude of neutrophilic rhinitis in this region between high-dose and repeated low-dose SG-exposed nasal passages (Figure 9).

Ultrastructural Alterations in the OE of SG-Exposed Nasal Passages

At the ultrastructural level, segments of olfactory nasal mucosa from the SG-exposed nasal passages exhibited a reduction in the number of OSN nuclear profiles in the middle layer of the OE, and a loss of OSN dendritic stereocilia lining the apical surface of the OE. Associated with this loss of normal OSN was

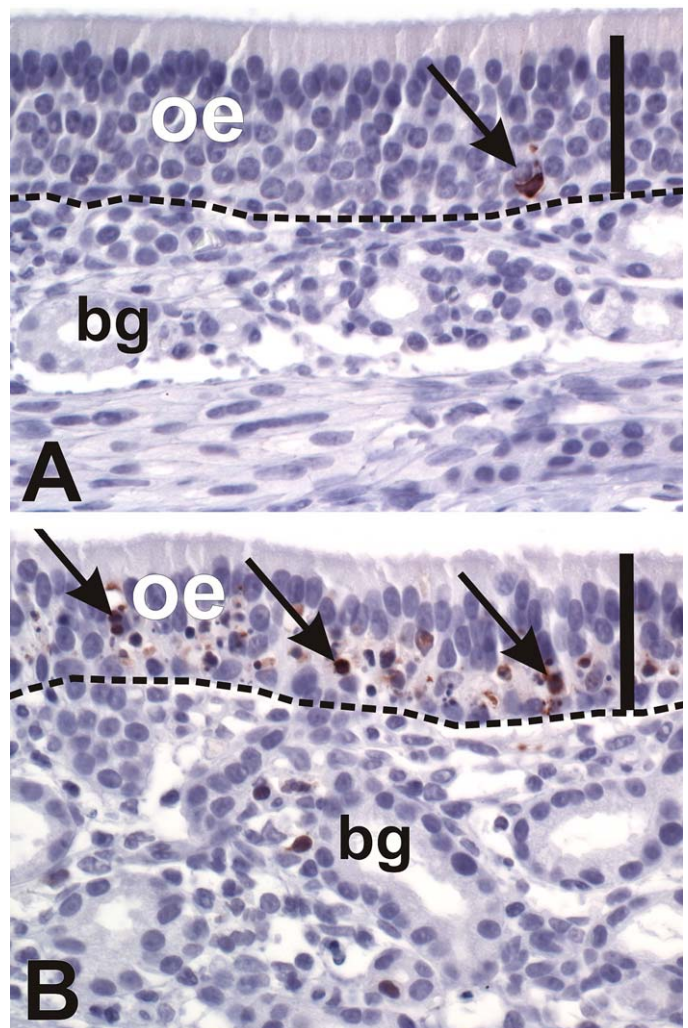


FIGURE 6.—Apoptosis of olfactory sensory neurons (OSN). (A, B) Light photomicrographs of olfactory epithelium (OE) lining the dorsal septum of a monkey treated with saline alone in the left nasal passage (A) and repeated low-dose SG in the right nasal passage (B). Sections were immunohistochemically stained for the pro-apoptotic protein caspase-3 (brown chromagen), and counterstained with hematoxylin. Note the low basal level of caspase-3 immunoreactivity detected in the saline-treated OE (A, arrow), compared to the increased detection of caspase-3 within the olfactory epithelium of the SG-treated nasal passage (B, arrows), indicating OSN apoptosis. Scale bar = 50 μm . bg = Bowman's glands.

the presence of electron dense apoptotic bodies in the middle third and basal layers of the OE (Figure 10), interspersed with the few remaining normal OSN nuclei. Neutrophils were present along the apical surface of affected OE, within the affected olfactory epithelium, and in the underlying lamina propria of the affected OE. Olfactory nasal mucosa from saline-exposed nasal passages did not exhibit any ultrastructural alterations.

DISCUSSION

In the present study, we have demonstrated that acute and repeated intranasal exposure to low doses of the black mold

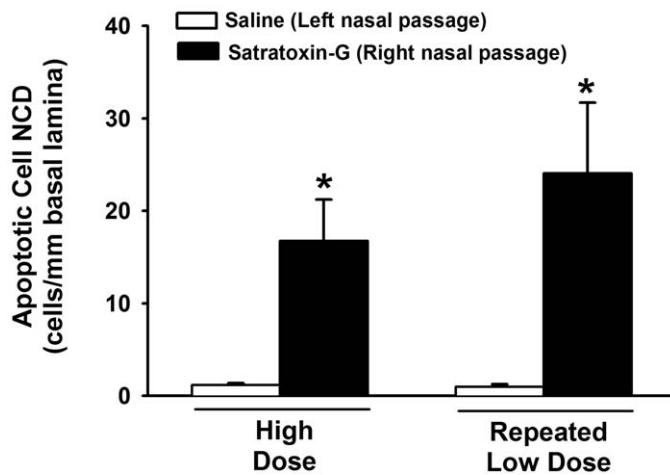


FIGURE 7.—Morphometric analysis of the numeric density of apoptotic cells within the OE lining the dorsal nasal septum of saline and SG-treated monkeys. * = significantly different from respective saline-treated group.

toxin SG induces widespread apoptosis of OSNs, olfactory epithelial and olfactory nerve atrophy, and acute neutrophilic rhinitis. Due to its proximal location in the respiratory tract and its function as a filter for inspired air, the nasal mucous membranes are susceptible to injury from inhaled air pollutants. SG is found in *S. chartarum* conidiospores and in fine, respirable fungal fragments in water-damaged environments (Brasel et al. 2005). Respiratory tract deposition of these particles is estimated to occur primarily in the extrathoracic portions of the respiratory system, including the nasal airways (Cheng 2003; Cho et al. 2005). For these reasons, the nasal airways are an important potential route of exposure to the black mold *S. chartarum* and its mycotoxins. Our observations demonstrate that the nasal airways of rhesus macaques, an animal model whose upper airways are structurally and functionally similar to those of humans, are vulnerable to injury induced by SG, and raise new questions about the potential hazards associated with exposure to *S. chartarum* in water-damaged environments.

Olfactory mucosal injury has been previously described in the nasal airways of laboratory mice following intranasal exposure to low doses of SG, as well as other macrocyclic trichothecene mycotoxins (Corps et al. 2010; Islam et al. 2007, 2006). In the present study, we used a comparable, low dose of SG (1 μg per nasal passage) to determine whether the olfactory mucosa of rhesus monkeys, a model for the nasal airways of people, exhibits similar vulnerability. We found that intranasal exposure to a low dose of SG evokes neutrophilic rhinitis and apoptosis of OSNs in monkeys, similar to the nasal injury reported in mice, suggesting that the nasal airways of laboratory rodents and nonhuman primates may exhibit similar vulnerability to the toxic effects of SG at comparable doses. It is important to note, however, that in previous studies in rodents, peak atrophy of the OE was observed at 3 days postinstillation, suggesting that the SG-exposed OE experiences ongoing loss of OSNs, along with a corresponding reduction in sustentacular cell

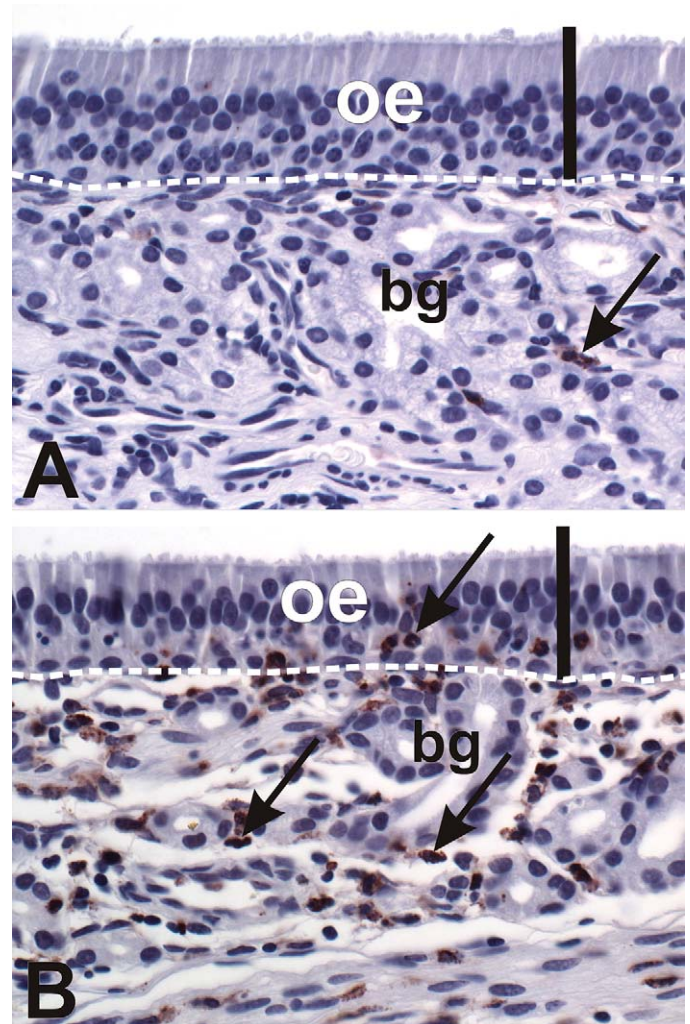


FIGURE 8.—Acute rhinitis in the nasal airways of SG-exposed monkeys. (A, B) Light photomicrographs of olfactory epithelium (OE) lining the dorsal septum of a monkey treated with saline alone in the left nasal passage (A) and repeated low-dose SG in the right nasal passage (B). Sections were immunohistochemically stained for the neutrophil enzyme myeloperoxidase. Note the influx of neutrophils (brown chromagen, arrows) in the epithelium and underlying lamina propria in the SG-exposed nasal passage in (B). Scale bar = 50 μm . bg = Bowman's glands.

height, for several days after exposure. In the present study, the nasal mucosa of SG-exposed monkeys was evaluated at 24 hours following the last exposure. Furthermore, since SG exposure also caused atrophy of the OE, the estimate of the volume fraction of OSNs used in this study will actually underestimate the total mass of OSNs lost following SG exposure. It is therefore likely that our study underestimates the peak toxic effect of SG on olfactory morphology.

While the responses of the olfactory mucosa to SG exposure were morphologically similar between mice and monkeys, they differ in their distribution. In the present study, all regions of OE in the monkey nasal cavity were affected by SG exposure, with the most extensive injury localized to the middle and

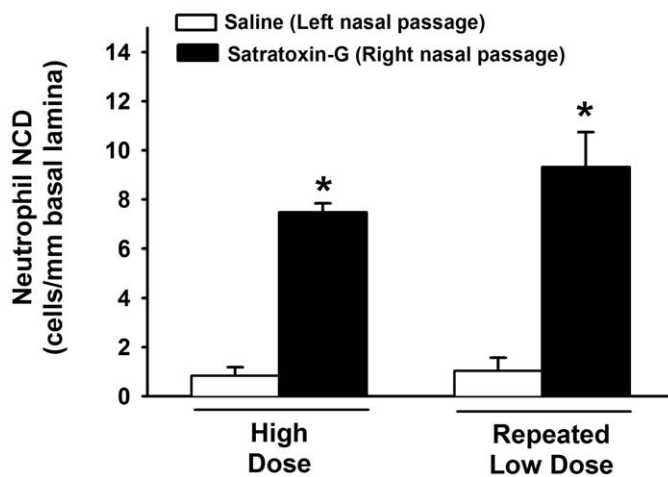


FIGURE 9.—Morphometric analysis of intraepithelial PMN numeric cell density in the OE lining the dorsal nasal septum. * = significantly different from respective saline-treated group.

dorsal nasal septum. In contrast, the OE lining the dorsal medial meatus of the mouse nasal cavity had no microscopic evidence of SG-induced injury (Islam et al. 2006). This same distribution of injury was also observed in mice following exposure to another macrocyclic trichothecene mycotoxin, roridin-A (Islam et al. 2007). One possible explanation for this interspecies variation is the difference in airflow patterns through the nasal airways of rodents and nonhuman primates. Computer-simulated estimates of inspiratory air flow patterns through the nasal airways indicate that the dorsal meatus is a site of high flow in the rodent nasal cavity (Kimbell et al. 1997) and a site of relatively low airflow in the rhesus monkey (Kepler et al. 1998) and in people (Hahn et al. 1993; Keyhani et al. 1995). The lower flows in the dorsal meatus of the rhesus monkey and people may facilitate aerosol particle deposition in that region. Another important difference is that the mice were exposed via intranasal instillation of a solution of SG in saline, while the monkeys were exposed intranasally to aerosolized SG with a microsyringe. While neither method precisely replicates exposure conditions for people, aerosolized particles and droplets are more representative of the nature of exposure in contaminated, water-damaged environments. Interestingly, despite the differences in nasal anatomy and dosing techniques, the neutrophilic rhinitis observed in both models was not widespread throughout the nasal airways but rather was strictly confined to the regions lined by olfactory mucosa. This distribution suggests that the inflammation in both species is a localized response to a specific interaction between the toxin and the olfactory mucosa, rather than a nonspecific response to the toxin or the administration.

One of the principal arguments against the hypothesis that *S. chartarum* causes adverse health effects in people is that the concentrations of *Stachybotrys* reported to cause toxicity in animal studies may not be achieved in water-damaged indoor air environments (Chapman et al. 2003; Hossain et al. 2004; Lai 2006). The total dose of SG used in the present study

(20 μg) would represent exposure to a large number of *Stachybotrys* spores (2×10^7) (Pestka et al. 2008), which may only be encountered in heavily contaminated areas (Brandt et al. 2006). However, SG is not only found in fungal spores, but is also present in viable and nonviable fungi and fungal fragments (Brasel et al. 2005). Airborne concentrations of these alternate sources of SG may be up to 500 times greater than airborne spore concentrations (Cho et al. 2005), making accurate estimates of indoor air concentrations and human exposure to SG difficult. Satratoxin-equivalent concentrations ranging from 2 to 330 ng/m^3 have been estimated to occur in rooms of water-damaged homes heavily contaminated with *S. chartarum* (Vesper et al. 2000; Yike et al. 1999). Acute, short-term exposure to high airborne concentrations of SG is likely to occur in heavily contaminated environments, or during processes that disrupt nutrient sources for mold, such as would occur during mold remediation procedures (Brandt et al. 2006). However, adverse health effects have also been associated with sustained or repeated exposure to damp indoor environments that are contaminated with *S. chartarum*, as would be expected in the workplace, home, or school (Park and Cox-Ganser 2011). Since the complete spectrum of possible exposures to *S. chartarum* and its mycotoxins remain poorly understood, it is important to consider the biological effects of exposure to *S. chartarum* and its mycotoxins via both acute exposure studies and chronic studies that use lower exposure concentrations (Institute of Medicine 2004). Here, we report that a single exposure to 20 μg of SG elicits rhinitis and OSN cell death in monkeys, and that exposure to a lower daily dose of SG (5 μg) for 4 consecutive days resulted in sustained rhinitis and more extensive OSN apoptosis and neuronal cell loss. Comparable effects of a single high dose and repeated low doses of SG in mice also indicated a cumulative effect of SG exposure (Islam et al. 2006). These findings suggest that the peak toxic effects associated with repeated SG exposures may be cumulative or delayed and stress the need for additional long-term exposure studies for better assessment of human risk.

Satratoxin levels in *Stachybotrys* conidiospores have been estimated to be 1 pg/spore (Pestka et al. 2008), suggesting that high levels of spores ($5\text{--}20 \times 10^6$) would be necessary to replicate the 5–20 μg doses used here. It should be recognized that in the environment SG would not exist as aerosolized droplet or gas, but rather in association with particulate, most notably spores (Brasel et al. 2005). Assuming each spore contains 1 pg of satratoxin and has a 5 μm diameter and spherical shape, the actual concentration of toxin within a conidiospore (based on volume) is 15 $\mu\text{g}/\text{cm}^3$. It might be speculated that if a spore becomes lodged within the nasal tract, the toxin concentration within its immediate microenvironment would be extremely high and capable of causing OSN apoptosis. Localized death could evoke punctate regions of cell loss within the olfactory epithelium. Furthermore, prolonged repeated low-level spore exposure could result in cumulative cell death, ultimately evoking reduced olfactory function. In support of this contention, following intranasal dosing of mice with SG (500 $\mu\text{g}/\text{kg}$ bw), the toxin selectively concentrates in nasal turbinates with levels

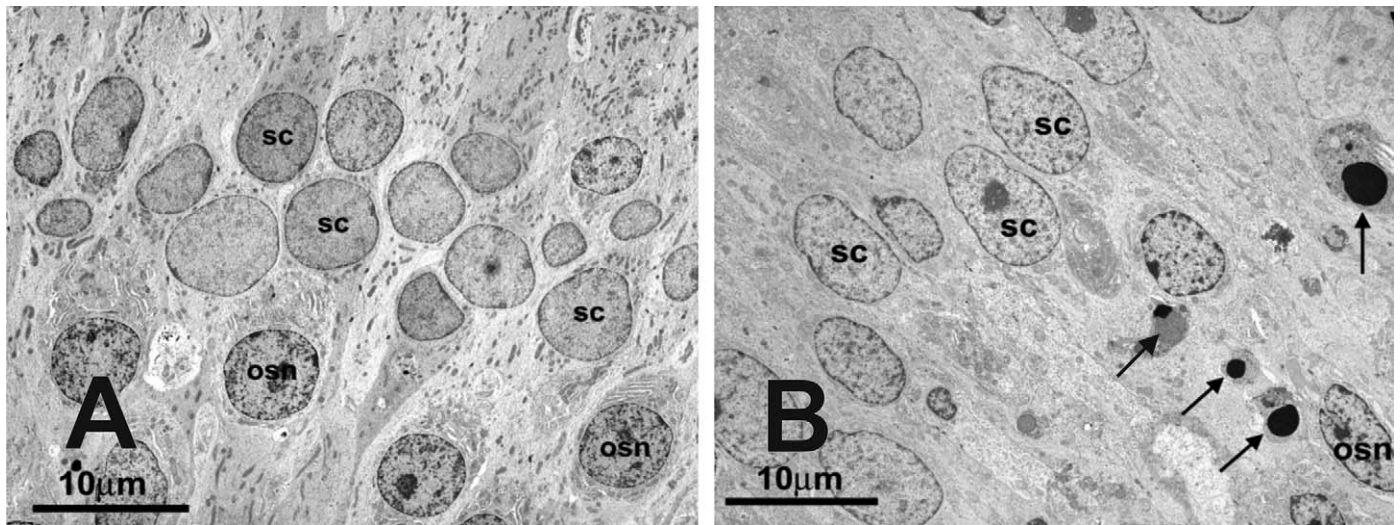


FIGURE 10.—Transmission electron photomicrographs of the middle third of the OE from a monkey treated with saline in the left nasal passage (A) and treated with repeated low-dose SG in the right nasal passage (B). Note the paucity of normal olfactory sensory neuron (OSN) nuclei and the presence of apoptotic bodies (arrows) through the middle third of the olfactory epithelium in (B). SC = sustentacular cells. Final magnification = 2,900X.

still being detectable after 24 h (Amuzie et al. 2010). It is further supported by our observation here that repeated daily intranasal exposure to SG at 5 μg over 4 days caused more extensive OSN damage in monkeys than that occurring from a single 20 μg dose. Further study is needed to determine the region-specific effects of repeated exposures to toxin-laden spores on the OE.

With this report, we demonstrate that intranasal exposure to the trichothecene mycotoxin SG evokes toxic epithelial injury and neuronal cell death in the nasal airways of rhesus monkeys. Due to the similarities in nasal structure and function between monkeys and humans, the use of a nonhuman primate model for nasal toxicity studies represents an important intermediate step in the extrapolation of data from rodent models for human risk assessment. However, the use of nonhuman primate models also presents several fundamental considerations, including the requirement for efficient and sound experimental design that allows the number of animals to be kept to a minimum (Smith and Boyd 2002). In our model, the use of a single nasal passage for SG exposure and the contralateral nasal passage for saline vehicle allowed each animal to serve as its own internal control, thereby reducing the number of animals required. The use of this model in future studies will facilitate the determination of whether toxicant-induced inflammation and neuronal cell death occur in the central nervous system of monkeys. The model will also be useful in evaluating therapies for this type of injury such as using ATP as described recently (Jia et al. 2011). Furthermore, by implementing neurobehavioral and neurocognitive test batteries, this model will provide the opportunity for the simultaneous evaluation of SG-induced airway toxicity, central nervous system injury, and behavioral and cognitive dysfunction (Capitanio and Emborg 2008; Golub 1990). By providing a pathologic link between SG exposure and central

nervous system dysfunction, studies employing the nonhuman primate model may address critical gaps in the association between exposure to damp buildings and reported neurologic symptoms.

While the present study stresses the critical importance of the nonhuman primate model for rigorous assessment of the human risk associated with exposure to *S. chartarum* in damp indoor environments, our results also emphasize the utility of the rodent model in the investigation of these potential health effects. Financial and regulatory limitations, among others, limit the utility of nonhuman primates in certain specific research endeavors (Lane 2000). The knowledge that intranasal exposure to SG in mice elicits morphologically similar nasal lesions to those observed in monkeys at comparable doses supports the use of laboratory mice in pharmacokinetic studies (Amuzie et al. 2010) and dose-response assessments of the toxic effects of SG and *S. chartarum*. These and other mechanistic assessments will be necessary for our understanding of how SG induces cell death and inflammation, as well as the basis for the specific targeting of OSNs.

Given the growing environmental health concerns of airborne fungi and their associated mycotoxins in water-damaged indoor environments, appropriate translational research is urgently needed to elucidate the potential health risks to people. In this report, we describe a novel nonhuman primate model of nasal airway and neuronal injury induced by intranasal exposure to the black mold toxin SG. Our observations that the nasal airways of monkeys are vulnerable to SG-induced neuronal cell death and inflammation is a critical step in our understanding of the potential health risks to people exposed to damp indoor environments, and the investigation of the potential etiologic role of *S. chartarum* in the pathogenesis of damp building-related illnesses. These data should

serve as the basis for future investigations using this model to determine whether intranasal SG exposure is capable of causing injury to the CNS, to determine the persistence of SG-induced olfactory system injury, and ultimately, to determine whether SG-induced nasal and neuronal injury are temporally associated with neurobehavioral and neurocognitive dysfunction. Finally, these morphologic and neurobehavioral endpoints in primates must be combined with mechanistic data from other species, and accurate exposure assessments in people to better predict human risk of adverse health effects from exposure to damp indoor environments.

ACKNOWLEDGMENTS

The authors thank Ms. Sarah Davis, Mr. Paul-Michael Sosa, Dr. Don Canfield, Ms. Sona Santos, Mr. Ralph Common, Ms. Kathy Joseph, Mr. Rick Rosebury, and Ms. Amy Porter for assistance with these experiments.

REFERENCES

- Amuzie, C. J., Islam, Z., Kim, J. K., Seo, J. H., and Pestka, J. J. (2010). Kinetics of satratoxin G tissue distribution and excretion following intranasal exposure in the mouse. *Toxicol Sci* **116**, 433–40.
- Andersson, M. A., M. Nikulin, U. Koljalg, M. C. Andersson, F. Rainey, K. Reijula, E. L. Hintikka and M. Salkinoja-Salonen (1997). Bacteria, molds, and toxins in water-damaged building materials. *Appl Environ Microbiol* **63**(2): 387–93.
- Brain, J. D. (1970). The uptake of inhaled gases by the nose. *Annals of Otolaryngology & Laryngology* **79**, 529–39.
- Brandt, M., Brown, C., Burkhardt, J., Burton, N., Cox-Ganser, J., Damon, S., Falk, H., Fridkin, S., Garbe, P., McGeehin, M., Morgan, J., Page, E., Rao, C., Redd, S., Sinks, T., Trout, D., Wallingford, K., Warnock, D., and Weissman, D. (2006). Mold prevention strategies and possible health effects in the aftermath of hurricanes and major floods. *MMWR Recomm Rep* **55**(RR-8), 1–27.
- Brasel, T. L., Douglas, D. R., Wilson, S. C., and Straus, D. C. (2005). Detection of airborne *Stachybotrys chartarum* macrocyclic trichothecene mycotoxins on particulates smaller than conidia. *Appl Environ Microbiol* **71**, 114–22.
- Capitanio, J. P., and Emborg, M. E. (2008). Contributions of non-human primates to neuroscience research. *Lancet* **371**, 1126–35.
- Carey, S. A., Minard, K. R., Trease, L. L., Wagner, J. G., Garcia, G. J. M., Ballinger, C. A., Kimbell, J. S., Plopper, C., Corley, R. A., Postlethwait, E. M., and Harkema, J. R. (2007). Three-dimensional mapping of ozone-induced injury in the nasal airways of monkeys using magnetic resonance imaging and morphometric techniques. *Toxicologic Pathology* **35**, 27–40.
- Chapman, J. A., Terr, A. I., Jacobs, R. L., Charlesworth, E. N., and Bardana, E. J., Jr. (2003). Toxic mold: phantom risk vs science. *Ann Allergy Asthma Immunol* **91**, 222–32.
- Cheng, Y. S. (2003). Aerosol deposition in the extrathoracic region. *Aerosol Science and Technology* **37**, 659–71.
- Cho, S.-H., Seo, S.-C., Schmechel, D., Grinshpun, S. A., and Reponen, T. (2005). Aerodynamic characteristics and respiratory deposition of fungal fragments. *Atmospheric Environment* **39**, 5454–65.
- Chung, Y. J., Jarvis, B., and Pestka, J. (2003). Modulation of lipopolysaccharide-induced proinflammatory cytokine production by satratoxins and other macrocyclic trichothecenes in the murine macrophage. *J Toxicol Environ Health A* **66**, 379–91.
- Corps, K. N., Islam, Z., Pestka, J. J., and Harkema, J. R. (2010). Neurotoxic, inflammatory, and mucosecretory responses in the nasal airways of mice repeatedly exposed to the macrocyclic trichothecene mycotoxin roridin A: dose-response and persistence of injury. *Toxicol Pathol* **38**, 429–51.
- Fog Nielsen, K. (2003). Mycotoxin production by indoor molds. *Fungal Genet Biol* **39**, 103–17.
- Fung, F., Clark, R., and Williams, S. (1998). *Stachybotrys*, a mycotoxin-producing fungus of increasing toxicologic importance. *J Toxicol Clin Toxicol* **36**, 79–86.
- Golub, M. S. (1990). Use of monkey neonatal neurobehavioral test batteries in safety testing protocols. *Neurotoxicol Teratol* **12**, 537–41.
- Gregory, L., Pestka, J. J., Dearborn, D. G., and Rand, T. G. (2004). Localization of satratoxin-G in *Stachybotrys chartarum* spores and spore-impacted mouse lung using immunocytochemistry. *Toxicol Pathol* **32**, 26–34.
- Gross, E. A., and Morgan, K. T. (1991). Morphometry of the nasal passages and larynx. In *Structural Diversity of the Mammalian Respiratory System: Comparative Morphology, Morphometry, Cytochemistry and Cellular Biology*. Boca Raton, FL, CRC Press.
- Hahn, I., Scherer, P. W., and Mozell, M. M. (1993). Velocity profiles measured for airflow through a large-scale model of the human nasal cavity. *Journal of Applied Physiology* **75**, 2273–87.
- Harkema, J. R., Carey, S. A., and Wagner, J. G. (2006). The nose revisited: a brief review of the comparative structure, function, and toxicologic pathology of the nasal epithelium. *Toxicol Pathol* **34**, 252–69.
- Hossain, M. A., Ahmed, M. S., and Ghannoum, M. A. (2004). Attributes of *Stachybotrys chartarum* and its association with human disease. *J Allergy Clin Immunol* **113**, 200–9.
- Hyde, D. M., Magliano, D. J., and Plopper, C. G. (1991). Morphometric assessment of pulmonary toxicity in the rodent lung. *Toxicol Pathol* **19**, 428–46.
- Hyde, D. M., Plopper, C., St. George, J. A., and Harkema, J. R. (1990). Morphometric cell biology of airspace epithelium. In *Electron Microscopy of the Lung* (D. E. Schraufnagel, ed.), pp. 1–120. New York, NY, Marcel Dekker.
- Institute of Medicine (2004). *Damp Indoor Spaces and Health*. C. o. D. I. S. a. Health. Washington, DC, Institute of Medicine of the National Academies.
- Islam, Z., Amuzie, C. J., Harkema, J. R., and Pestka, J. J. (2007). Neurotoxicity and inflammation in the nasal airways of mice exposed to the macrocyclic trichothecene mycotoxin roridin a: kinetics and potentiation by bacterial lipopolysaccharide coexposure. *Toxicol Sci* **98**, 526–41.
- Islam, Z., Harkema, J. R., and Pestka, J. J. (2006). Satratoxin G from the black mold *Stachybotrys chartarum* evokes olfactory sensory neuron loss and inflammation in the murine nose and brain. *Environ Health Perspect* **114**, 1099–107.
- Jia, C., Sangsiri, S., Belock, B., Iqbal, T., Pestka, J. J., and Hegg, C. C. (2011). ATP mediates neuroprotective and neuroproliferative effects in mouse olfactory epithelium following exposure to satratoxin G in vitro and in vivo. *Toxicol Sci* **124**(1): 169–78.
- Kepler, G. M., Richardson, R. B., Morgan, K. T., and Kimbell, J. S. (1998). Computer simulation of inspiratory nasal airflow and inhaled gas uptake in a rhesus monkey. *Toxicology and Applied Pharmacology* **150**, 1–11.
- Keyhani, K., Scherer, P. W., and Mozell, M. M. (1995). Numerical simulation of airflow in the human nasal cavity. *J Biomech Eng* **117**, 429–41.
- Kilburn, K. H. (2004). Role of molds and mycotoxins in being sick in buildings: neurobehavioral and pulmonary impairment. *Adv Appl Microbiol* **55**, 339–59.
- Kimbell, J. S., Godo, M. N., Gross, E. A., Joyner, D. R., Richardson, R. B., and Morgan, K. T. (1997). Computer simulation of inspiratory airflow in all regions of the F344 rat nasal passages. *Toxicology & Applied Pharmacology* **145**, 388–98.
- Kream, R., and Margolis, F. (1984). Olfactory marker protein: turnover and transport in normal and regenerating neurons. *The Journal of Neuroscience* **4**, 868–79.
- Lai, K. M. (2006). Hazard identification, dose-response and environmental characteristics of *stachybotryotoxins* and other health-related products from *Stachybotrys*. *Environ Technol* **27**, 329–35.
- Lane, M. A. (2000). Nonhuman primate models in biogerontology. *Experimental Gerontology* **35**, 533–41.
- Park, J. H., and Cox-Ganser, J. M. (2011). Mold exposure and respiratory health in damp indoor environments. *Front Biosci (Elite Ed)* **3**, 757–71.
- Pestka, J. J., Yike, I., Dearborn, D. G., Ward, M. D., and Harkema, J. R. (2008). *Stachybotrys chartarum*, trichothecene mycotoxins, and damp building-

- related illness: new insights into a public health enigma. *Toxicol Sci* **104**, 4–26.
- Plopper, C. G., Chu, F. P., Haselton, C. J., Peake, J., Wu, J., and Pinkerton, K. E. (1994). Dose-dependent tolerance to ozone. I. Tracheobronchial epithelial reorganization in rats after 20 months' exposure. *American Journal of Pathology* **144**, 404–20.
- Smith, J. A., and Boyd, K. M. (2002). *The Boyd Group Papers on the Use of Non-Human Primates in Research and Testing*. Leicester, UK, British Psychological Society.
- Tuomi, T., Reijula, K., Johnsson, T., Hemminki, K., Hintikka, E. L., Lindroos, O., Kalso, S., Koukila-Kahkola, P., Mussalo-Rauhamaa, H., and Haahtela, T. (2000). Mycotoxins in crude building materials from water-damaged buildings. *Appl Environ Microbiol* **66**, 1899–904.
- Vesper, S., Dearborn, D. G., Yike, I., Allan, T., Sobolewski, J., Hinkley, S. F., Jarvis, B. B., and Haugland, R. A. (2000). Evaluation of *Stachybotrys chartarum* in the house of an infant with pulmonary hemorrhage: quantitative assessment before, during, and after remediation. *J Urban Health* **77**, 68–85.
- Yang, G. H., Jarvis, B. B., Chung, Y. J., and Pestka, J. J. (2000). Apoptosis induction by the satratoxins and other trichothecene mycotoxins: relationship to ERK, p38 MAPK, and SAPK/JNK activation. *Toxicol Appl Pharmacol* **164**, 149–60.
- Yike, I., Allan, T., Sorenson, W. G., and Dearborn, D. G. (1999). Highly sensitive protein translation assay for trichothecene toxicity in airborne particulates: comparison with cytotoxicity assays. *Appl Environ Microbiol* **65**, 88–94.
- Yike, I., and Dearborn, D. G. (2004). Pulmonary effects of *Stachybotrys chartarum* in animal studies. *Adv Appl Microbiol* **55**, 241–73.
- Yike, I., Rand, T. G., and Dearborn, D. G. (2005). Acute inflammatory responses to *Stachybotrys chartarum* in the lungs of infant rats: time course and possible mechanisms. *Toxicol Sci* **84**, 408–17.

For reprints and permissions queries, please visit SAGE's Web site at <http://www.sagepub.com/journalsPermissions.nav>.